ELSEVIER

Journal of Biomechanics 38 (2005) 1283–1290

JOURNAL OF BIOMECHANICS

www.elsevier.com/locate/jbiomech
www.JBiomech.com

Combined effects of pulsatile flow and dynamic curvature on wall shear stress in a coronary artery bifurcation model

I.V. Pivkin[a], P.D. Richardson[b], D.H. Laidlaw[c], G.E. Karniadakis[a,*]

[a]*Division of Applied Mathematics, Center for Fluid Mechanics, 182 George Street, Box F, Providence, RI 02912, USA*
[b]*Division of Engineering, Brown University, RI, USA*
[c]*Department of Computer Science, Brown University, RI, USA*

Accepted 20 June 2004

Abstract

A three-dimensional model with simplified geometry for the branched coronary artery is presented. The bifurcation is defined by an analytical intersection of two cylindrical tubes lying on a sphere that represents an idealized heart surface. The model takes into account the repetitive variation of curvature and motion to which the vessel is subject during each cardiac cycle, and also includes the phase difference between arterial motion and blood flowrate, which may be nonzero for patients with pathologies such as aortic regurgitation. An arbitrary Lagrangian Eulerian (ALE) formulation of the unsteady, incompressible, three-dimensional Navier–Stokes equations is employed to solve for the flow field, and numerical simulations are performed using the spectral/hp element method. The results indicate that the combined effect of pulsatile inflow and dynamic geometry depends strongly on the aforementioned phase difference. Specifically, the main findings of this work show that the time-variation of flowrate ratio between the two branches is minimal (less than 5%) for the simulation with phase difference angle equal to 90°, and maximal (51%) for 270°. In two flow pulsatile simulation cases for fixed geometry and dynamic geometry with phase angle 270°, there is a local minimum of the normalized wall shear rate amplitude in the vicinity of the bifurcation, while in other simulations a local maximum is observed.

Keywords: Hemodynamics; Atherosclerosis; Coronary arteries; Wall shear stress; Bifurcation; Pulsatile flow; Curved tube model

1. Introduction

It is widely believed that the development and progression of atherosclerosis is related to the complex flow field occurring in curvatures and bifurcations of large and medium arteries (Caro et al., 1971; Ku et al., 1985; Friedman et al., 1987). Numerical studies based on rigid, idealized (Steinman et al., 2000; Bertolotti and Deplano, 2000) as well as realistic geometries (Myers et al., 2001; Steinman et al., 2002; Zeng et al., 2003) have been useful in understanding the unique complex features of these flows. Most of these investigations focus on the effects of the geometry, pulsatile flow and non-Newtonian behavior of blood in non-moving vessels. Perktold and Rappitsch (1995) and Zhao et al. (2000) analyzed the effect of distensible wall on the local flow field. Some authors have suggested that the flexibility and motion of coronary artery during each contraction and expansion of the heart is important in the study of the flow dynamics. Several investigations used models in which the vessel was represented by a single flexible tube (Schilt et al., 1996; Santamarina et al., 1998; Zeng et al., 2003).

Comparatively less is known about the effects of vessel movement on the blood flow patterns in coronary arteries at *bifurcations*. Zeng et al. (2003) simulated a realistic arterial motion based on biplane cineangiograms

*Corresponding author. Fax: +1-401-863-3369.
E-mail address: gk@cfm.brown.edu (G.E. Karniadakis).

0021-9290/$ - see front matter © 2004 Elsevier Ltd. All rights reserved.
doi:10.1016/j.jbiomech.2004.06.015

in human right coronary arteries but did not consider any branches. Weydahl and Moore (2001) were among the first to consider the model of coronary artery at bifurcation with time-varying geometry. They showed that curvature variation is important in determining temporal wall shear stress variations. However, they considered only steady inflow.

The objective of the present work is to analyze the *combined effect* of dynamic geometry and pulsatile inflow on the flow dynamics and wall shear rate in a simple model of a coronary artery at bifurcation. This will allow us to take into account any *phase difference* between the two unsteady phenomena that may arise in cardiac disease.

Normal coronary flow velocities are characterized by a small forward flow during systole and a large forward flow during diastole (Guyton, 1986). In cardiac disease other patterns can arise. For example, if there is an infarcted region of myocardium, the cardiac muscle in that region does not contract as healthy muscle. Consequently, the epicardial blood flow variation and the deformations of the ventricular wall masses may both change. If the infarct is due to current thrombotic obstruction, outflow resistance in the corresponding intramural segments is not relieved in diastole. Matsuo et al. (1988) have connected the change in phasing information to aortic regurgitation. Using a bidirectional Doppler flowmeter catheter to examine coronary flow velocity in patients who had aortic valve disease, they found a decreased diastolic and increased systolic coronary flow. In some cases, the diastolic flow velocity was less than the systolic. These flow velocity patterns became notable with severe aortic regurgitation. Such phenomena have a direct effect on the *phase difference* between the arterial motion studied here and the pulsatile inflow imposed in our models.

While approximate values for epicardial artery curvature and its variation through a heartbeat are known, precise values are problematic to obtain. Biplane or multiplane angiograms taken in vivo are useful for estimating the axes of vessel segments through the cardiac cycle but do not register lumenal diameters or details sufficiently accurately, and do not show artery wall tissue characteristics. Intravascular ultrasound can supply lumenal geometry and wall tissue information but does not of itself find vessel curvature, takes some time to generate in vivo, and is limited to larger-diameter coronary vessels. MRI, while potentially providing geometric information and wall structure details for coronary arteries, is still not at a state-of-art where spatial resolution is as good as desired for the present study. Thus, to explore fluid dynamic features of curvature variation as well as curvature and flow pulsatility we have chosen to examine flow in a branched vessel model with prescribed but representative parameter values.

2. Basic assumptions

A three-dimensional bifurcating model is defined by an analytical intersection of two cylindrical tubes lying on a sphere that represents an idealized heart surface (Fig. 1). Due to the sharp edge at the junction of arterial branches the solution has a numerical singularity that is localized in a small region close to the junction and does not seem to affect the results in other parts of the domain. The heart motion is simulated by changing the sphere radius, R; the center of the sphere is fixed at the coordinate origin. Gross and Friedman (1998) obtained the dynamics of coronary artery curvature from biplane cineangiograms. The results of this study suggest significant harmonic content up to 6 Hz in curvature variation, and this was taken into account in the numerical studies of Weydahl and Moore (2001) and Moore et al. (2001). Here we have adopted the same range of parameters as in Weydahl and Moore (2001) and Moore et al. (2001), i.e. we take the frequency of the sphere radius variation to be 5 Hz, so that the period $T = 0.2$ s. More specifically, R is specified as a sinusoidal function

$$R(t) = R_0(1 + \delta \sin(2\pi t/T)),$$

where the mean sphere radius R_0 is set to 56.25 mm. Three different values of the parameter δ were used in simulations, 0.0, 0.1 and 0.3. In addition, two cases were considered with $\delta = 0.0$ and R equal to 50.625 and 61.875 mm, i.e., minimum and maximum radii for the dynamic case with $\delta = 0.1$.

The tubes have a circular cross section with constant diameters $D_1 = 3$ mm and $D_2 = 1.5$ mm. At time $t = 0$, the length of the segments AB, BC and BD are equal to 10.125, 24.0 and 12.375 mm, respectively. The lengths of arterial segments are fixed in time so that the total volume of the model remains constant. The junction angle θ is 45°, which is different from the bifurcation modeled in Weydahl and Moore (2001). The axis of the large tube is located in the xy-coordinate plane while the small tube is in the $z > 0$ half-space. The point of intersection of the tube axes B lies on the x-coordinate axis during the entire cardiac cycle. The blood is assumed to be an incompressible, Newtonian

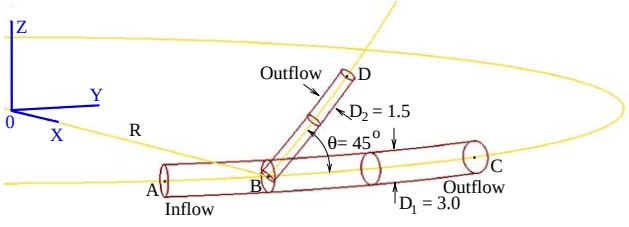

Fig. 1. Geometry of the bifurcation and coordinate system (dimensions in mm).

and homogeneous fluid. The flow is three-dimensional and unsteady, and the Reynolds number defined by $Re = D_1 U_0/\nu$ is 300, where U_0 is the mean inflow velocity (Weydahl and Moore, 2001).

3. Methods and verification

The three-dimensional, unsteady, incompressible Navier–Stokes equations are cast in an arbitrary Lagrangian Eulerian (ALE) frame and solved using the parallel solver NEKTAR that employs the new generation of spectral/hp element methods (Karniadakis and Sherwin, 1999). The mesh, constructed using the commercially available mesh generator Gridgen (Pointwise, Inc.), has 6649 tetrahedral elements (Fig. 2). The initial domain corresponds to the model geometry with sphere radius $R = R_0$. The advantage of the ALE formulation in conjunction with the high-order interpolants employed in the spectral/hp element method is that the simulation can be run *without remeshing*.

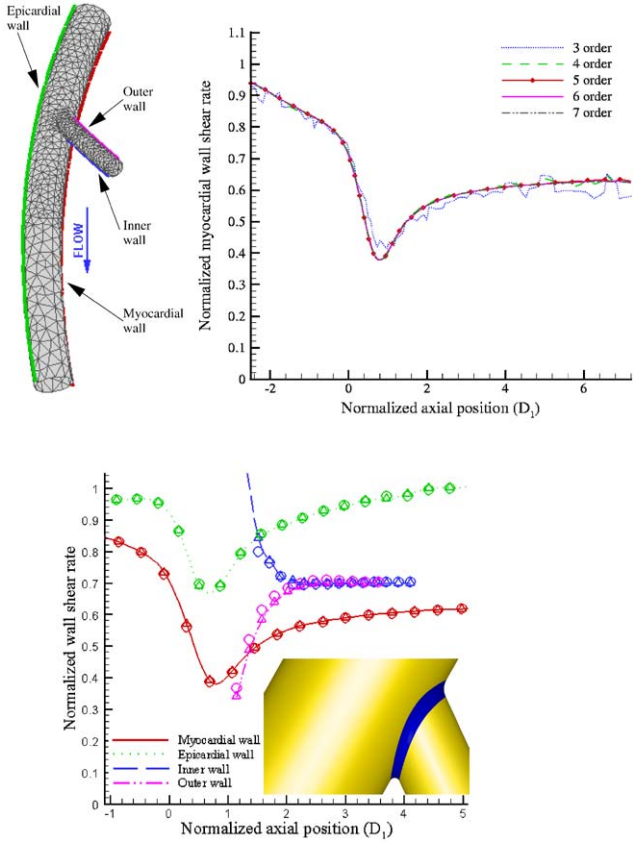

Fig. 2. Upper: wall shear rate versus polynomial order (p-refinement) for the reference case ($\delta = 0.0, \varepsilon = 0.0$). The wall shear rate is extracted along the myocardial wall and normalized by the magnitude of the wall shear rate in a straight pipe with the same diameter and Reynolds number. The distance is measured from the inter-section point of the tube axes (point B in Fig. 1) and normalized by the large tube diameter D_1. Lower: the normalized wall shear rate extracted along selected lines on the myocardial and epicardial walls of the main branch, and the inner and outer walls of the side branch: sharp edge geometry at junction with side branch (triangles), smoothed edge geometry at the same location (circles).

To characterize the coronary blood flow velocities, we use a simple time-dependent sinusoidal function with frequency matching the geometry variation frequency. More specifically, at the *inflow* the pulsatile flat velocity profile is specified as

$$U(t) = U_0\left(1 + \varepsilon \sin\left(2\pi t/T + \frac{\alpha\pi}{180}\right)\right).$$

The mean inflow velocity U_0 is 400 mm/s (Weydahl and Moore, 2001). Note that here, we allow for a phase difference α degrees between the flowrate and the arterial motion; we will systematically investigate this difference for four different values of α in the next section. The parameter ε is set to 0 for simulations with constant inflow velocity; in pulsatile cases, ε is set to 0.1 or 0.3 (Folkow and Neil, 1971). At the two *outflow* sections (main and side branch) a constant (equal) pressure and zero normal derivatives of velocity are imposed; no-slip conditions are used at the vessel walls.

To ensure mesh independence of the computational results, several resolution studies were performed. The mesh was fixed at a position with the sphere radius $R = R_0$. The resolution was then increased by increasing the polynomial expansion order in each element, i.e. by p-refinement (Fig. 2). In all simulations described below, fifth-order ($p = 5$) polynomial expansion was used uniformly for all elements.

To estimate the effect of the sharp edge at the junction we have performed a simulation with the edge smoothed using the following procedure. The side branch tube was intersected with the tube that has the same axis as the main tube and 10% larger radius. The irrelevant part of the side branch tube was removed. Similar manipulations were done with the main tube. The radius of the intersecting tube in this case was 20% larger than side branch tubes radius. The two disjoint tube segments were connected with a smooth surface. The obtained geometry at the junction is shown in Fig. 2. The results of the simulations for the sharp and smooth edge models with fixed geometry and steady inflow show that the difference in wall shear rate in regions that are used for analysis further in the paper is less than 5%; it is maximum on the surface of the side branch (Fig. 2).

The time-step independence of the results was verified for the case with dynamic curvature variation ($\delta = 0.1$) and pulsatile inflow ($\varepsilon = 0.1$). The time step was divided by two and the computational results were compared against those with the original time step; no differences were found. To obtain a time-periodic solution the simulations were run for three time periods, $3T$, and the last period taken.

Table 1
Summary of cases simulated.

δ	0.0	0.1	0.0	0.1	0.1	0.1	0.1	0.1 min*	0.1 max*	0.3	0.0	0.3	0.3
ε	0.0	0.0	0.1	0.1	0.1	0.1	0.1	0.0	0.0	0.0	0.3	0.3	0.3
α (deg)	0	0	0	0	90	180	270	0	0	0	0	0	180

Here δ corresponds to the normalized amplitude variation of the dynamic curvature radius and ε to the inflow velocity variation.

4. Results

We have summarized the cases we have simulated in Table 1. In the two cases marked with $*$, the geometry was fixed at the minimum and maximum radii for the dynamic case with $\delta = 0.1$, which correspond to $R = 50.625$ and 61.875 mm, respectively. Next, we present the main results for representative cases only.

4.1. Velocity field and secondary flow structure

In most simulations, the main flow features are quite similar to the results with steady inflow and static geometry ($\varepsilon = 0.0$ and $\delta = 0.0$). The core of the flow in the main branch is shifted towards the epicardial wall. There is a Dean-type vortex structure in the main branch, which is typically seen in flows in curved tubes (Fig. 3, upper row). The fluid moves from the myocardial wall to the epicardial along the diameter, and then returns to the myocardial wall along the sides of the tube, forming two counter-rotating vortices. The vortical structures are symmetric before one large tube diameter D_1 from the point of intersection of tube axes. The presence of a side branch results in vortex skewing and loss of symmetry, that can be seen up to three large tube diameters beyond the bifurcation. The shift of the flow core towards the epicardial wall in the main branch produces an overall rotating fluid motion in the side branch beyond the bifurcation, that soon disappears due to viscous forces (not shown here). Similar flow patterns were observed by Sherwin et al. (2000) for the flow within a distal end-to-side anastomosis with non-planar geometry. The secondary flow is weak in the side branch (about four small tube diameters from the bifurcation), and counter-rotating vortices are hardly seen. The dynamic geometry changes the secondary flow structure. Here we show the results for the simulation case with parameters $\delta = 0.3$ and $\varepsilon = 0.0$ (Fig. 3, lower row). The oscillation of the vortical structures in the main branch during the simulation cycle is apparent in the figure.

4.2. Flowrate through the branches

The dynamic geometry and pulsatile inflow affect the flow distribution between the two branches of the model

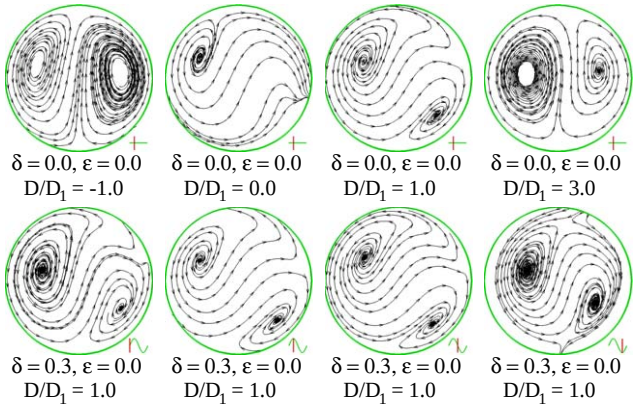

Fig. 3. Secondary flow structure (cross-flow streamlines) for two simulation cases. Upper row: reference (steady) case, fixed geometry and steady inflow ($\delta = 0.0, \varepsilon = 0.0$). Lower row: unsteady case, dynamic geometry and steady inflow ($\delta = 0.3, \varepsilon = 0.0$). The cross-sections are taken perpendicular to the tube axes at different times during the periodic cycle and at certain distances from the inter-section point of axes of main and side branches. The distance is normalized by the large (D_1) tube diameter. The flow is out of the page and the bifurcation point is at $D/D_1 = 0.0$. The cross-sections are plotted with the epicardial wall on the top and the myocardial wall on the bottom; the side branch wall is located on the right.

(Fig. 4). All simulations show a *phase difference* between the variation of curvature or inflow velocity and the flowrate ratio variation. In the simulation with fixed averaged geometry and steady inflow, the flowrate ratio between the side and the main branch is 0.123. Both dynamic geometry and pulsatility can result in more than 20% change in the flowrate ratio. The difference in flowrate through the side branch is insignificant in quasi-static simulations, when the geometry is fixed with mean, minimum or maximum curvature radii. The combined effect of dynamic geometry and pulsatile inflow depends strongly on the phase difference angle α. In the simulation with $\alpha = 90^\circ$ the variation is the least of all the simulations (less than 5%). The maximum variation, observed for $\alpha = 270^\circ$, is 51%.

4.3. Wall shear rate

Next, we examine the distribution of the wall shear rate (WSR) at selected cross-sections of the main and side branch. The extracted values of the WSR are

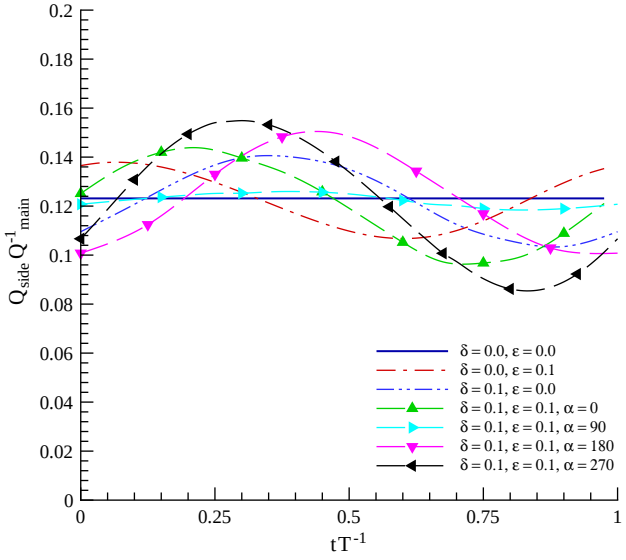

Fig. 4. Variation of the flowrate ratio between the main (Q_{main}) and side (Q_{side}) branch during the periodic cycle for different simulations.

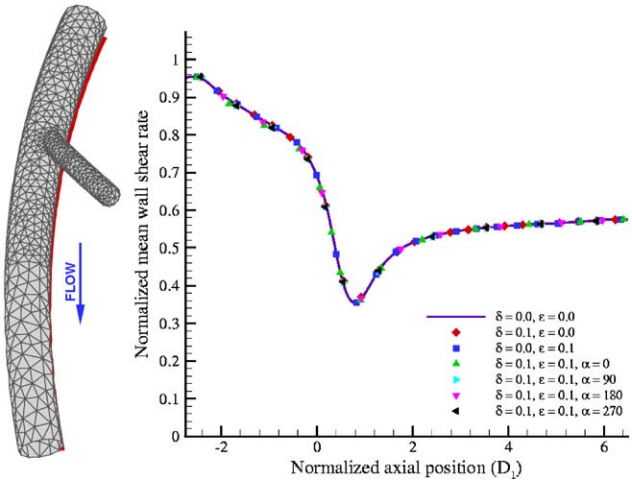

Fig. 5. Normalized *time-averaged* wall shear rate extracted along the myocardial wall for different simulation cases.

normalized by the magnitude of the wall shear rate in a straight pipe with the same diameter and Reynolds number. The same normalization of the WSR is used for all results presented here. For the simulation with steady inflow and fixed (in the mean) position geometry ($\delta = 0.0, \varepsilon = 0.0$), the highest WSR values occur on the side branch wall of the main branch beyond the bifurcation. In general, the WSR is lower on the myocardial wall of the main branch than on the epicardial wall. Low WSR values are also observed on the outer wall of the side branch close to bifurcation. The effect of curvature on the WSR distribution is not pronounced in the side branch. The time-averaged WSR is similar to the steady inflow and fixed geometry case (Fig. 5). This is consistent with previous findings in Weydahl and Moore (2001) and Zeng et al. (2003), but somewhat surprising for the combined cases considered here due to the large temporal variation, especially for certain values of the phase difference, as we see next.

The WSR variations along the myocardial wall of the main branch in simulation with dynamic geometry and steady inflow ($\delta = 0.1, \varepsilon = 0.0$) are significant in comparison to its low mean (Fig. 6). The region of the largest WSR variation during the cycle is located on the surface of the side branch and can be attributed to the significant variation of the flowrate through the branch. The variation of WSR during the cycle in simulation with fixed geometry and pulsatile inflow ($\delta = 0.0, \varepsilon = 0.1$) is large in comparison to the previously described case. This is in agreement with the results of Zeng et al. (2003) for a single coronary artery without a side branch. In our case, this can be related to the temporal variation of the total mass flow through the model.

Next, we compare the combined effect of pulsatility ($\varepsilon = 0.1$) and unsteady geometry ($\delta = 0.1$) with phase difference $\alpha = 0^\circ, 90^\circ, 180^\circ$ and 270° on mean (i.e., time-averaged) values and variation of WSR during the periodic cycle (Fig. 7). In the main branch, the dependence of WSR variation on the phase difference is less pronounced before the bifurcation than after. For the simulation cases with $\alpha = 90^\circ$ and 180°, the variation of WSR before the bifurcation in the main branch is larger on the myocardial wall than on the epicardial. The opposite is observed in simulations with $\alpha = 0^\circ$ and 270°. One large tube diameter beyond the bifurcation in the main branch, both minimal and maximal variations of WSR are observed in simulation with phase difference of 270°. More specifically, the minimum is located on the myocardial wall and the maximum on the side branch wall. At the same time, maximal WSR variation on the myocardial wall and minimal WSR variation on the side branch wall are observed in the simulation with $\alpha = 90^\circ$. The magnitude of the time-dependent WSR on the myocardial wall becomes very low during the periodic cycle in this simulation. Further beyond the bifurcation, the dependence of WSR variation on the phase difference becomes less pronounced. In the side branch, the overall WSR variation depends strongly on α. Minimal variation is observed when $\alpha = 90^\circ$ and maximal variation when $\alpha = 270^\circ$. In the latter case, the minimum of the magnitude of the WSR on the outer wall of the side branch during the periodic cycle is very low.

4.4. Combined effect of δ, ε and α on NWSRA

In general, in all simulations an increase of parameters δ and ε produces a linear increase in the variation of wall shear rate. To characterize WSR variation during the cycle we use the normalized wall shear rate amplitude (NWSRA). This quantity was introduced in

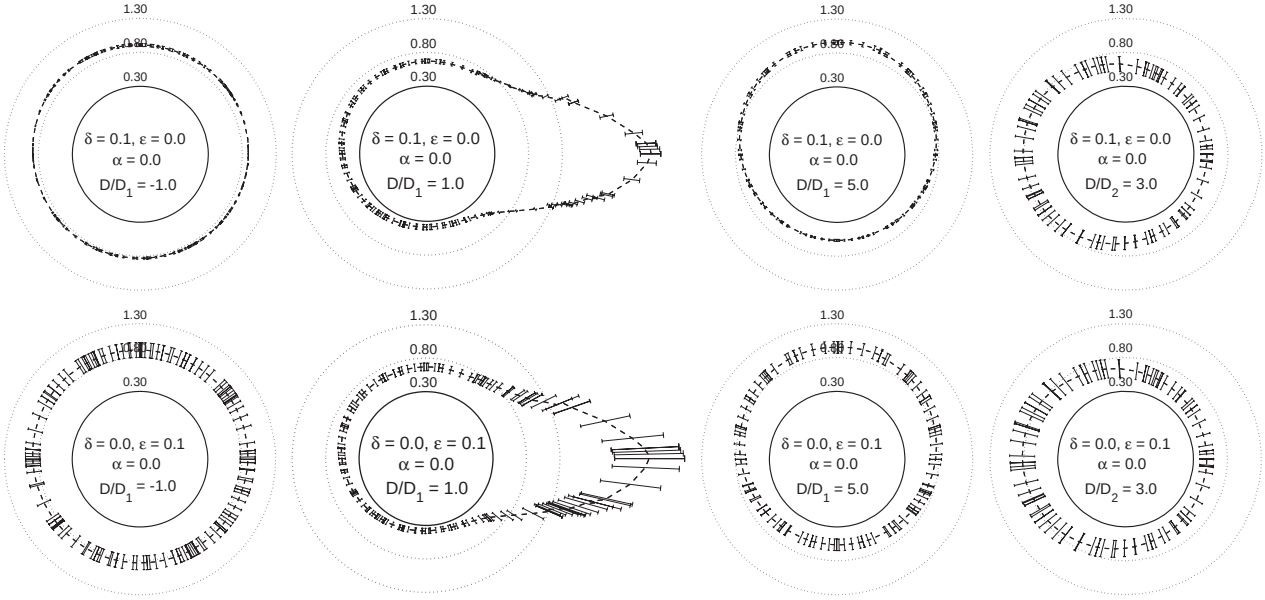

Fig. 6. Wall shear rate, mean (time-averaged), and variation during the periodic cycle. Upper row: the case with dynamic geometry and steady inflow ($\delta = 0.1, \varepsilon = 0.0$). Lower row: effect of pulsatile inflow on WSR ($\delta = 0.0, \varepsilon = 0.1$). The cross-sections are taken perpendicular to the tube axes at certain distances from the intersection point of axes of main and side branches. The distance is normalized by the large (D_1) or small (D_2) tube diameter for the main or side branch cross-sections, respectively. The extracted values of the WSR are normalized by the magnitude of the wall shear rate in a straight pipe with the same diameter and Reynolds number.

Santamarina et al. (1998) and was also used in Weydahl and Moore (2001), since it may be more relevant to atherogenesis research than the dimensional WSR amplitudes, which are of more interest from a fluid dynamics perspective. NWSRA is defined as the difference between the maximum and minimum values of the WSR during the cycle divided by the mean ($\delta = 0.0, \varepsilon = 0.0$) WSR.

Next we examine the combined effect of curvature, inflow velocity and phase difference variations on NWSRA along the myocardial wall of the main branch (Fig. 8). We can subdivide this figure into three regions. The first region corresponds to the part of the myocardial wall located before the tube axes intersection point (zero on the horizontal axis in the figure). The second region extends from this point up to three large tube diameters and the third region includes the rest of the figure. In the first and third regions the main contribution to the NWSRA is from the pulsatility of the flow. The dependence of the NWSRA on the phase difference α is strong and can change the results even qualitatively, as shown in the figure for region two. In general, in the second region, the dependence of the NWSRA on the simulation parameters is less intuitive. In two simulation cases, ($\delta = 0.0, \varepsilon = 0.1, \alpha = 0^\circ$) and ($\delta = 0.1, \varepsilon = 0.1, \alpha = 270^\circ$), the distribution of NWSRA differs significantly from the other cases: there is a local minimum approximately 0.9 large tube diameters below the tube axes intersection, while in other simulations a local maximum is observed.

5. Summary and conclusions

We have presented new results on the effects of unsteady flow in an unsteady (flexing) geometry—a side-branched, curved tube flexing rhythmically in curvature—as an approximation of the flows in and motions of epicardial coronary arteries. These results go further than the recent study of Zeng et al. (2003), which lacked a side branch, and the earlier study of Weydahl and Moore (2001), which included a side branch but lacked flow pulsatility. The tube geometry, the flexing motion and the flow pulsations are all approximations of what happens in physiological and pathological circumstances. Such investigations help in determining which boundary conditions have such significant effects that they should be included in any study where, say, the flow pulsations include more than the fundamental frequency in a Fourier decomposition. We found that the flowrate ratio between the side branch and the main branch is influenced significantly by the combined unsteady phenomena, as is the wall shear rate distribution in the vicinity of the bifurcation.

Our results demonstrate the importance of phase difference, not previously modeled in computational studies. While the effects of curvature and of flexing well away from bifurcation region agree reasonably with straightforward expectations and previous studies, the effects of phase difference are particularly marked in the close vicinity of the bifurcation and in regard to the wall shear rate of the flow. As the latter is widely

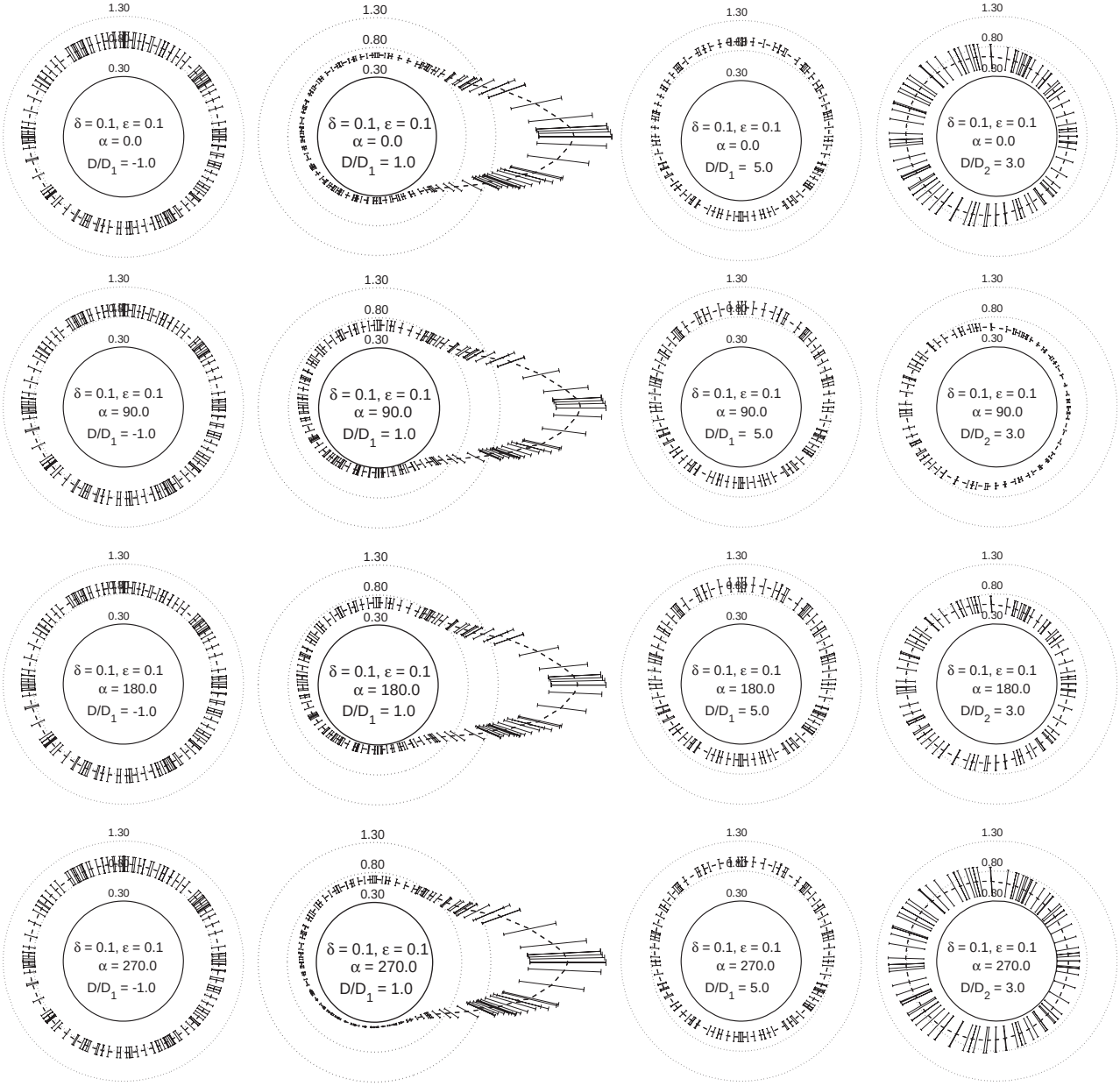

Fig. 7. Wall shear rate, mean (time-averaged) and variation (bars) during the periodic cycle. Results are shown for the cases with dynamic geometry ($\delta = 0.1$) and pulsatile inflow ($\varepsilon = 0.1$) for phase difference angles $\alpha = 0^\circ, 90^\circ, 180^\circ, 270^\circ$. The cross-sections are taken perpendicular to the tube axes at certain distances from the intersection point of axes of main and side branches. The distance is normalized by the large (D_1) or small (D_2) tube diameter for the main or side branch cross-sections, respectively. The extracted values of the WSR are normalized by the magnitude of the wall shear rate in a straight pipe with the same diameter and Reynolds number. The cross-sections are plotted with the epicardial wall on the top and the myocardial wall on the bottom. For the main branch cross-sections, the side branch wall is located on the right. For the side branch cross-sections, the inner wall is located on the left and the outer wall on the right. The circles represent the gridlines for values 0.3 (solid), 0.8 and 1.3 (dotted).

hypothesized to influence atherosclerosis and its sequelae, this makes arterial flexure and its phase difference from the flow important for more refined studies to include.

The role and significance of the phase angle α may be considered by first considering the variation of R with respect to the cardiac cycle. To zeroth approximation, the radius R increases as the ventricles are filled with blood (diastole), and R decreases as blood ventricular pressure is raised and blood is expelled (systole). Diastole begins around 270°. In a healthy heart, then, α might be in the vicinity of 180°. Matsuo et al. (1988) have shown that with some pathologies, such as aortic regurgitation or aortic stenosis, the effective phase of flow in the coronaries can be shifted from normal. These pathologies, of course, are not of the coronary arteries

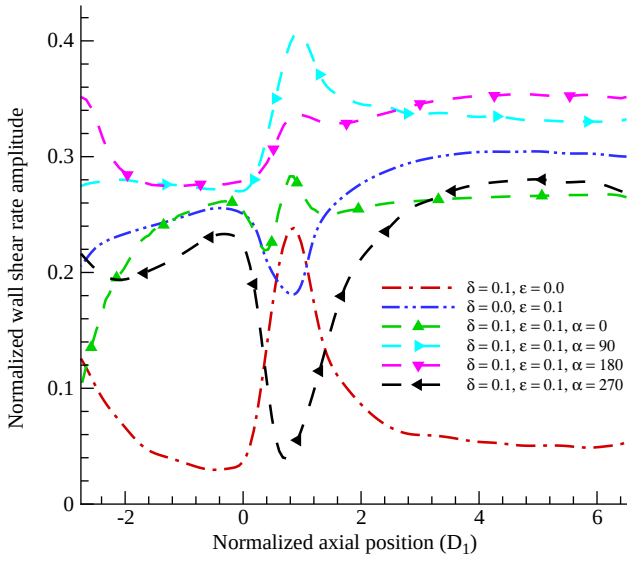

Fig. 8. Normalized wall shear rate amplitude (NWSRA) extracted along the myocardial wall for different simulation cases.

themselves. However, in view of our results which show alterations of the wall shear stress distribution around a major bifurcation with change in α (the value of ε might also be changed by the pathologies), to the extent that atherosclerosis and plaque development are affected by local flow conditions including wall shear stress distribution, we can propose as a hypothesis that specific pathologies (aortic regurgitation or aortic stenosis) outside the coronary arteries may have an influence on the atherosclerotic developments in those arteries. This hypothesis lacked a mechanistic basis before the computational results we present here.

Acknowledgements

This work was supported by an NSF-ITR Grant (CCR-0086065) and by BSF (IBSF 2001150). We would like to thank S.J. Sherwin of Imperial College and Z. Yosibash and A. Yakhot of Ben Gurion University for useful discussions. Computations were performed on the AHPCC Los Lobos Linux cluster.

References

Bertolotti, C., Deplano, V., 2000. Three-dimensional numerical simulations of flow through a stenosed coronary bypass. Journal of Biomechanics 33 (8), 1011–1022.

Caro, C.G., Fitz-Gerald, J.M., Schroter, R.C., 1971. Atheroma and arterial wall shear. Observation, correlation and proposal of a shear dependent mass transfer mechanism for atherogenesis. Proceedings of the Royal Society of London B Biological Sciences 177 (46), 109–159.

Folkow, B., Neil, E., 1971. Circulation. Oxford University Press, New York.

Friedman, M.H., Bargeron, C.B., Deters, O.J., Hutchins, G.M., Mark, F.F., 1987. Correlation between wall shear and intimal thickness at a coronary artery branch. Atherosclerosis 68 (1–2), 27–33.

Gross, M.F., Friedman, M.H., 1998. Dynamics of coronary artery curvature obtained from biplane cineangiograms. Journal of Biomechanics 31 (5), 479–484.

Guyton, A.C., 1986. Textbook of Medical Physiology, 7th ed. Saunders, Philadelphia.

Karniadakis, G.E., Sherwin, S.J., 1999. Spectral/hp element methods for CFD. Numerical Mathematics and Scientific Computation. Oxford University Press, New York.

Ku, D.N., Giddens, D.P., Zarins, C.K., Glagov, S., 1985. Pulsatile flow and atherosclerosis in the human carotid bifurcation. Positive correlation between plaque location and low oscillating shear stress. Arteriosclerosis 5 (3), 293–302.

Matsuo, S., Tsuruta, M., Hayano, M., Imamura, Y., Eguchi, Y., Tokushima, T., Tsuji, S., 1988. Phasic coronary-artery flow velocity determined by doppler flowmeter catheter in aortic-stenosis and aortic regurgitation. American Journal of Cardiology 62 (13), 917–922.

Moore, J.E., Weydahl, E.S., Santamarina, A., 2001. Frequency dependence of dynamic curvature effects on flow through coronary arteries. Journal of Biomechanical Engineering—Transactions of the ASME 123 (2), 129–133.

Myers, J.G., Moore, J.A., Ojha, M., Johnston, K.W., Ethier, C.R., 2001. Factors influencing blood flow patterns in the human right coronary artery. Annals of Biomedical Engineering 29 (2), 109–120.

Perktold, K., Rappitsch, G., 1995. Computer-simulation of local blood-flow and vessel mechanics in a compliant carotid-artery bifurcation model. Journal of Biomechanics 28 (7), 845–856.

Santamarina, A., Weydahl, E., Siegel, J.M., Moore, J.E., 1998. Computational analysis of flow in a curved tube model of the coronary arteries: effects of time-varying curvature. Annals of Biomedical Engineering 26 (6), 944–954.

Schilt, S., Moore, J.E., Delfino, A., Meister, J.J., 1996. The effects of time-varying curvature on velocity profiles in a model of the coronary arteries. Journal of Biomechanics 29 (4), 469–474.

Sherwin, S.J., Shah, O., Doorly, D.J., Peiro, J., Papaharilaou, Y., Watkins, N., Caro, C.G., Dumoulin, C.L., 2000. The influence of out-of-plane geometry on the flow within a distal end-to-side anastomosis. Journal of Biomechanical Engineering—Transactions of the ASME 122 (1), 86–95.

Steinman, D.A., Poepping, T.L., Tambasco, M., Rankin, R.N., Holdsworth, D.W., 2000. Flow patterns at the stenosed carotid bifurcation: effect of concentric versus eccentric stenosis. Annals of Biomedical Engineering 28 (4), 415–423.

Steinman, D.A., Thomas, J.B., Ladak, H.M., Milner, J.S., Rutt, B.K., Spence, J.D., 2002. Reconstruction of carotid bifurcation hemodynamics and wall thickness using computational fluid dynamics and MRI. Magnetic Resonance in Medicine 47 (1), 149–159.

Weydahl, E.S., Moore, J.E., 2001. Dynamic curvature strongly affects wall shear rates in a coronary artery bifurcation model. Journal of Biomechanics 34 (9), 1189–1196.

Zeng, D.H., Ding, Z.H., Friedman, M.H., Ethier, C.R., 2003. Effects of cardiac motion on right coronary artery hemodynamics. Annals of Biomedical Engineering 31 (4), 420–429.

Zhao, S.Z., Xu, X.Y., Hughes, A.D., Thom, S.A., Stanton, A.V., Ariff, B., Long, Q., 2000. Blood flow and vessel mechanics in a physiologically realistic model of a human carotid arterial bifurcation. Journal of Biomechanics 33 (8), 975–984.